

JGR Solid Earth

RESEARCH ARTICLE

10.1029/2022JB024622

Key Points:

- Teleseismic *P*-wave tomography is used in combination with anisotropy models to study the origin of the low-velocity anomalies below the Moroccan Atlas
- We incorporate anisotropy as an *a priori* constraint in tomography and show the reduction in low-velocity anomalies below the Moroccan Atlas
- The lateral travel of plume material from the Canary Hotspot may be the origin of low-velocity anomalies

Supporting Information:

Supporting Information may be found in the online version of this article.

Correspondence to:

H. Lee,
leex8217@umn.edu;
leex8217@snu.ac.kr

Citation:

Lee, H., Bezada, M. J., & Kim, Y. (2022). The origin of the low-velocity anomalies beneath the rootless Atlas Mountains: Insights gained from modeling of anisotropy developed by the travel of Canary Plume. *Journal of Geophysical Research: Solid Earth*, 127, e2022JB024622. <https://doi.org/10.1029/2022JB024622>

Received 19 APR 2022




Accepted 8 NOV 2022

Author Contributions:

Conceptualization: Hwaju Lee, Maximiliano J. Bezada, YoungHee Kim
Formal analysis: Hwaju Lee, Maximiliano J. Bezada, YoungHee Kim
Funding acquisition: Hwaju Lee, Maximiliano J. Bezada, YoungHee Kim
Investigation: Hwaju Lee, Maximiliano J. Bezada, YoungHee Kim
Methodology: Maximiliano J. Bezada
Software: Maximiliano J. Bezada
Supervision: Maximiliano J. Bezada, YoungHee Kim
Validation: Maximiliano J. Bezada
Visualization: Hwaju Lee
Writing – original draft: Hwaju Lee
Writing – review & editing: Hwaju Lee, Maximiliano J. Bezada, YoungHee Kim

© 2022. American Geophysical Union.
All Rights Reserved.

The Origin of the Low-Velocity Anomalies Beneath the Rootless Atlas Mountains: Insights Gained From Modeling of Anisotropy Developed by the Travel of Canary Plume

Hwaju Lee^{1,2} , Maximiliano J. Bezada¹ , and YoungHee Kim² 

¹School of Earth & Environmental Sciences, University of Minnesota, Minneapolis, MN, USA, ²School of Earth and Environmental Sciences, Seoul National University, Seoul, Republic of Korea

Abstract As the mantle plume rises from the deep mantle and reaches the base of a tectonic plate, it changes its traveling direction from vertical to horizontal. The horizontal spread of plume material is often radially asymmetric. An example is a plume found below the Canary Hotspot. Previous studies have suggested that the channeling of the Canary Plume toward the westernmost Mediterranean (Alboran Sea) and consequent lithospheric delamination may have contributed to the low-velocity anomalies found beneath the Moroccan Atlas Mountains. Regional upwelling and edge-driven convection have been proposed as other candidates to explain the origin of the low-velocity anomalies. In this study, we incorporated anisotropy as an *a priori* constraint in teleseismic *P*-wave travel-time tomography as mantle flow can develop seismic anisotropy. We inverted a new set of travel-time delays by removing the hypothetical anisotropy-imposed travel-time delays from the observations. Our improved results are more consistent with the hypothesis that the low-velocity anomalies come from the mantle material of the Canary Plume.

Plain Language Summary The propagation velocity of seismic waves is sensitive to the temperature. Low seismic velocities in the mantle found from seismic tomography, a technique used to image the velocity structure of the inner Earth with seismic waves, are commonly interpreted as high-temperature, hydrous regions, the presence of partial melting, changes in the compositional chemistry, and grain sizes of mantle minerals. Thus, seismic tomography has been the primary tool for revealing mantle structures, such as hot plumes rooted in the deep mantle that play significant roles in mantle dynamics. Previous studies have shown that rising plume material can drag the surrounding mantle and consequently cause directional dependence of the seismic velocities, which can also affect the results of seismic tomography. This study improved the quality of seismic tomography results by considering the directional dependence of wave speeds in the mantle to elucidate the evolution of the mantle plume and its interaction with the upper plate in Morocco. The imaged low-velocity conduit below the high-altitude Moroccan Atlas indicates the lateral travel of the mantle plume originating from the Canary Hotspot in northwest Africa, which may have dragged the surrounding mantle beneath the Moroccan Atlas.

1. Introduction

Since Wilson (1963) suggested the existence of mantle plumes to explain the Hawaiian island chain, the vertical rise of buoyant material from the deep mantle and consequent decompression melting near the surface have been considered a mechanism for the formation of hotspots (e.g., Morgan, 1971; Sleep, 1990). The buoyancy of the hot mantle primarily originates from temperature. Therefore, there have been many attempts to better constrain the mantle plume structure using seismic tomography as the high-temperature mantle is imaged as low-seismic-velocity anomalies (e.g., DePaolo & Manga, 2003; French & Romanowicz, 2015; Humphreys et al., 2000; Montelli et al., 2006; Nolet et al., 2007; Ritter et al., 2001; Zhao, 2007). When the plume reaches the base of a plate, it must deflect its direction of travel from vertical to sub-horizontal (e.g., Ihinger, 1995; Kerr & Lister, 2008; Ribe & Christensen, 1994; Richards & Griffiths, 1988; Thoraval et al., 2006). However, the horizontal spread of the plume is not always radially symmetric. Instead, previous studies have suggested that plume material can be dragged by or can drag the surrounding mantle in its direction of flow (e.g., Ito et al., 2014; Ribe & Christensen, 1994, 1999; Richards & Griffiths, 1988; Sleep, 1990; Thoraval et al., 2006). Consequently, this lateral travel of the mantle plume can extend hundreds to thousands of kilometers while producing magmatism and the developing (sea) mountain systems on the upper plate. For instance, based on geophysical and

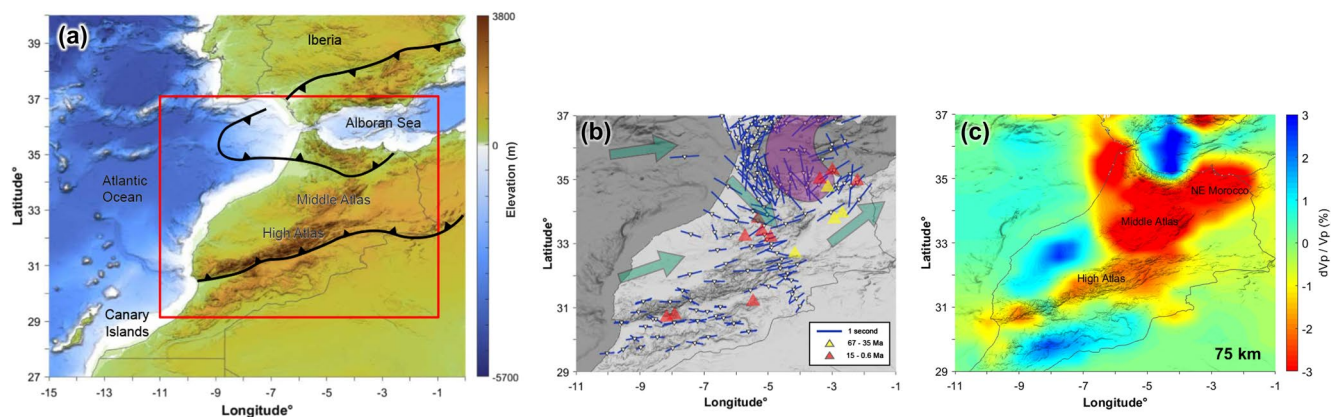


Figure 1. (a) Physiographic features of the regional map. Black lines with sawteeth show the location of the thrust faults. The solid-red box presents the area shown in panels (b) and (c). (b) The observation of shear wave splitting (SWS) (Diaz et al., 2010; Miller et al., 2013) at stations (white inverted triangles). The length of the blue bar indicates the SWS time while the orientation represents the fast polarization direction. The yellow and red triangles show the approximated location of volcanoes that erupted during 67–35 and 15–0.6 Ma, respectively (Teixell et al., 2005). The green arrows present the proposed mantle flow followed by Figure 7 of Diaz et al. (2010) and the purple area presents the location of the high-velocity Alboran slab (Bezada et al., 2013). (c) The depth slice of isotropic *P*-wave tomography image at 75 km for the study region. It shows low-velocity anomalies across the Moroccan Atlas and northeast Morocco. The black-dashed box indicates the region used in the analysis of this study.

geochemical data, it has been proposed that the Afar and Réunion hot plumes flow along sub-lithospheric channels horizontally (or laterally) beneath East Africa and Arabia (near the Red Sea) (e.g., Bagley & Nyblade, 2013; Chang & Van der Lee, 2011; Hansen et al., 2012) and the western Indian Ocean (e.g., Barruol et al., 2019; Füre et al., 2011; Morgan, 1978; Sleep, 2008), respectively. The lateral travel of mantle plume material from the Juan Fernández hotspot was suggested to explain low-velocity anomalies at depths greater than 100 km beneath the Nazca Plate in Chile (e.g., Portner et al., 2017). The lateral channeling of the plume from the 70-million-year-old Canary Hotspot Islands, 100 km offshore of the western coast of Morocco (28°N, 16°W), toward the westernmost Mediterranean (Alboran Sea) has also been suggested as the origin of the low-velocity anomalies beneath Morocco (Duggen et al., 2009; Miller et al., 2015). Alternatively, edge-driven convection (EDC), “baby” mantle plume (small-scale mantle plume), and delamination-initiated local upwelling have been suggested as their origin (Kaislaniemi & van Hunen, 2014; Missenard & Cadoux, 2012; Missenard et al., 2006; Teixell et al., 2005). Utilizing teleseismic *P*-wave travel-time tomography, this study examines various scenarios that try to explain the origin of low-velocity anomalies, in the lithosphere including lateral channeling of Canary Plume material. At the same time, it also explores the effect of anisotropy produced in these various hypothetical scenarios on tomographic imaging.

1.1. Tectonic Framework of the Moroccan Atlas and Its Deep Structure

The High and Middle Atlas Mountains (Atlas Mountains) are an intra-continental mountain range that extends from the Atlantic coast of southwest Morocco to the northeastern border between Morocco and Algeria (Figure 1a). Although it is not at a convergent boundary, the Atlas Mountain is one of the highest mountain ranges in Africa. The mountains formed as a result of the inversion of Triassic-Jurassic age grabens when Africa converged with Eurasia during the Cenozoic (Arbolea et al., 2004; Brede et al., 1992; Gomez et al., 1998; Piqué et al., 2002; Teixell et al., 2003). However, the estimated tectonic shortening due to compression during the Eocene and Pliocene-Quaternary is not sufficient to support the topography of the Atlas (e.g., Beauchamp et al., 1999; Frizon de Lamotte et al., 2000; Fullea et al., 2007, 2008; Gomez et al., 1998; Teixell et al., 2003, 2009). Previous studies have suggested (a) the absence of a deep crustal root (Ayarza et al., 2005; Miller & Becker, 2014; Missenard et al., 2006; Sandvol et al., 1998) or (b) thinned lithosphere beneath mountains (Anahnah et al., 2011; Ayarza et al., 2005; Civiero et al., 2018; Miller & Becker, 2014; Missenard et al., 2006; Sun et al., 2014; Teixell et al., 2003, 2005; Timoulali et al., 2019; Zeyen et al., 2005). Detailed geophysical investigations have revealed low-velocity anomalies in the upper mantle below the mountains (e.g., Bezada et al., 2014; Calvert et al., 2000; Civiero et al., 2018, 2019; Fullea et al., 2010; Miller et al., 2015; Palomeras et al., 2014; Seber et al., 1996; Timoulali et al., 2015). These investigations conclude that buoyancy of the underlying hot mantle supports the

Table 1
Summary of Anisotropy Models

Model name	UpW	EDC	Lateral	OneStem	TwoStems
Representing hypothesis for the origin of the hot mantle	(1) Lithospheric delamination (2) Activation of a baby plume	Edge-driven convection	Mantle material from the Canary Plume		
Consistency with the observed SWS	×	×	✓	✓	✓
Spatial distribution (shape)	The distribution of low-velocity anomalies slower than 2% dVp/Vp				
Depth distribution	60–160 km		60–160 km except for the upwelling stems at 160–200 km		
Anisotropy field	To reproduce one second (mean of observed delay time within the study area)				

high topography of the mountains rather than a crustal root. The presence of a hot mantle coincides at the surface with intra-plate alkali Cenozoic magmatism in Morocco (Figure 1b) (Anguita & Hernán, 2000; Lustrino & Wilson, 2007; Teixell et al., 2005). The first pulse of volcanic activity took place at 67–35 Ma (Figure 1b, yellow triangles) and the second pulse, which is much more voluminous, took place at 15–0.6 Ma (Figure 1b, red triangles).

Thermal erosion of the lithosphere has been proposed to explain the origin of the hot mantle as well as the loss of the lithosphere beneath the mountains, but there is no consensus on the detailed mechanism driving this process. Current hypotheses (Table 1) include: (a) crustal thickening and consequent mantle upwelling after the delamination (Ramdani, 1998), (b) activation of a baby plume (Fullea et al., 2010; Lustrino & Wilson, 2007), (c) development of small-scale EDC in the mantle between the West African Craton and Atlas lithosphere (i.e., warm mantle upwelling beneath the Atlas mountains and mantle downwelling adjacent to the edge of the craton) (Fullea et al., 2010; Kaislaniemi & van Hunen, 2014; Manjón-Cabeza Córdoba & Ballmer, 2021; Missenard & Cadoux, 2012), and (d) travel of mantle material from the Canary Plume (28°N, 16°W), which may have removed the base of the lithosphere below the Atlas (Anguita & Hernán, 2000; Duggen et al., 2009; Miller & Becker, 2014; Miller et al., 2015; Sun et al., 2014). Perhaps, the travel of Canary Plume material toward the Alboran Sea and consequent lithospheric delamination are more consistent with the geochemical analysis (Anguita & Hernán, 2000; Duggen et al., 2009; Lustrino & Wilson, 2007) and shear wave splitting (SWS) observations (Buontempo et al., 2008; Diaz et al., 2010; Miller & Becker, 2014; Miller et al., 2013). The geochemical analysis of mafic lavas from the Middle Atlas demonstrated that they share similar geochemical properties with those from the Canary Islands (Anguita & Hernán, 2000; Duggen et al., 2009). Duggen et al. (2009) further suggested that mantle suction due to the westward rollback of the Alboran slab (i.e., decompressed mantle above the slab) found beneath the Alboran Sea may have become a driving force for the lateral travel of mantle plume material. Meanwhile, based on waveform modeling, Sun et al. (2014) suggested the presence of a low-velocity column beneath the Middle Atlas that Miller et al. (2015) later interpreted as one of the uprising vertical plume conduits, which would have branched out from the Canary Plume, based on results from receiver function analysis. More recent tomographic results suggest that the low-velocity structure found in the lithosphere below the Atlas Mountains is connected to the Canary Plume beneath the transition zone (Civiero et al., 2018, 2021).

1.2. Seismic Anisotropy Evidenced by SWS Observations

The observation of SWS based on dense seismic coverage in Morocco and its vicinity provides clear evidence for seismic anisotropy in the region (Buontempo et al., 2008; Diaz et al., 2010; Miller & Becker, 2014; Miller et al., 2013). The observed delay time (dt) is <1 s in the High Atlas and gradually increases to ~2 s in north-east (NE) Morocco (the northern coast of Morocco near Gibraltar Arc). Previous studies have suggested that toroidal mantle flows around the subducted Alboran Slab contributed to the SWS observations in the region of NE Morocco (Civiero et al., 2019; Diaz et al., 2010; Faccenda & Capitanio, 2012, 2013; Lee et al., 2021). The observed fast polarization directions (FPD) of the Middle and High Atlas are generally oriented SW-NE, whereas the FPD of NE Morocco is oriented in an arcuate shape along the coast of the Alboran Sea (Figure 1b).

(Diaz et al., 2010, 2015; Miller et al., 2013). The predominant source of seismic anisotropy inferred from the SWS data is the lattice-preferred orientation (LPO) of olivine in the mantle. As mantle flow can develop LPO, investigating seismic anisotropy provides useful insights into the direction of the mantle flow (e.g., Christensen, 1984; Fouch & Rondenay, 2006; Ismail & Mainprice, 1998; Silver, 1996).

At the same time, seismic anisotropy can influence seismic travel times and be imaged as velocity anomalies (e.g., Bezada et al., 2016; Blackman & Kendall, 1997; Eberhart-Phillips & Henderson, 2004; Ishise & Oda, 2005; Lloyd & Van der Lee, 2008; Wu & Lees, 1999). When mantle rocks experience shear stress, the seismically fast direction (SFD) of A-type olivine (a-axis) aligns subparallel to the direction of maximum shear (the direction of mantle flow) (e.g., Anderson, 1989; Hirth & Kohlstedt, 2003; Ismail & Mainprice, 1998; Kaminski & Ribe, 2002; Tommasi et al., 1999). As a result, assuming a simplified hexagonal symmetry for olivine anisotropy, the mantle with the SFD aligned subparallel to the surface (or plate) (aligned perpendicular to the traveling direction of teleseismic rays) can be imaged as low-velocity anomalies. Conversely, the mantle with the SFD aligned perpendicular to the surface (or plate) (aligned parallel to the traveling direction of teleseismic rays) can be imaged as high-velocity anomalies. For sub-horizontal orientations of the LPO, seismic anisotropy can be mapped in isotropic tomography as low-velocity anomalies that are added to the effect of temperature and composition (Bezada et al., 2016; Faccenda & Capitanio, 2012; Hu et al., 2017; Kaminski & Ribe, 2002; Lee et al., 2021).

Thus, having the observations of SWS as a piece of evidence for seismic anisotropy in the study region and taking it as a proxy for LPO of A-type olivine developed by mantle flow, we include five different anisotropy structures in the tomography that represent various hypotheses for the origin of the low-velocity anomalies found beneath the Atlas Mountains. As different configurations of mantle flow are expected based on the hypotheses suggested for the region, considering different seismic anisotropy structures may shed light on the origin of the low-velocity anomalies found in the lithosphere of the study region. Furthermore, we attempted to examine the contribution of seismic anisotropy to the *P*-wave low-velocity anomalies found beneath Morocco (Figure 1c), which previous studies have interpreted as mantle material with excessive temperature or partial melt.

2. Data and Method

The isotropic model is the same as the one used by Bezada et al. (2014). We used the tomographic inversion method and the data set of Bezada et al. (2014), which utilized 76,524 travel-time delays from 332 events recorded by 398 stations in the Iberian Peninsula and Morocco (inverted triangles in Figure 1b and Figure S1 in Supporting Information S1). Travel-time delays were determined by multi-channel cross-correlation (VanDecar & Crosson, 1990) in three frequency bands (0.3, 0.5, and 1.0 Hz). These delays were inverted for tomographic inversion using the hybrid ray-tracing method introduced by Bezada et al. (2013), which combines iterative ray tracing and finite-frequency kernels. Ray tracing inside the velocity model is carried out by accounting for the 3D structure using a method based on graph theory (Hammond & Toomey, 2003; Toomey et al., 1994). The outside of the modeled volume is 1D. At depths above ~80 km, we implemented the surface wave tomography model of Palomeras et al. (2014) as a starting model. Further details of isotropic tomography and its related synthetic tests can be found in Bezada et al. (2013, 2014).

Isotropic inversion for volumetric body-wave tomography is an ill-posed and non-unique problem, as the earthquakes (sources) and seismic stations (receivers) are unevenly distributed (i.e., some nodes of the tomographic models are under-determined while others are over-determined). To stabilize the inversion, regularization methods such as damping and smoothing are often applied, and this leads to trade-offs between data misfit and complexity of structure in the tomographic model. Considering anisotropy in tomography inversion is further challenging since it requires the inversion of direction and magnitude of anisotropy for each node, even when hexagonal symmetry of anisotropy is assumed (Fouch & Rondenay, 2006; Huang et al., 2015; Maupin & Park, 2007; Trampert, 1998). Although anisotropic tomography is possible (e.g., Eberhart-Phillips & Henderson, 2004; VanderBeek & Faccenda, 2021; Zhao et al., 2016), since introducing anisotropy in tomographic inversion introduces more unknowns into an already underdetermined problem, isotropic tomographic inversions are still preferentially carried out at various scales. In this study, instead of performing a full anisotropic inversion, we include a series of hypothetical anisotropy model as an *a priori* constraints in the isotropic inversion. This is accomplished by performing forward travel-time calculations that take into account the chosen anisotropic structure (see Hammond & Toomey, 2003 for methodological details). This essentially includes the anisotropy in the reference

model so that the effect of the chosen anisotropy field is removed from the travel-time delays that are inverted for isotropic velocity perturbations. The *a priori* anisotropy field is held constant for all iterations. Using synthetic and real data, Bezada et al. (2016) and Lee et al. (2021) showed that this approach is a functional alternative to full anisotropic inversion.

3. Anisotropy Models

We accommodated the various hypotheses suggested by previous studies on the origin of low-velocity anomalies (hot mantle) beneath the Atlas Mountains into five simple-yet-representative anisotropy models (Section 1.1, Table 1): regional upwelling (UpW), EDC, lateral conduit (Lateral), OneStem (lateral conduit with one local upwelling stem below the Middle Atlas), and TwoStems (lateral conduit with two local upwelling stems below the Middle Atlas and NE Morocco).

3.1. Hypotheses for the Origin of the Low-Velocity Anomalies and the Corresponding Orientation of SFD of the Anisotropy Models

3.1.1. Regional Upwelling (UpW)

We would expect all of the SFD to be aligned vertically (perpendicular to the surface) as the direction of the mantle flow is upward and/or downward whether the origin of the low-velocity anomalies found beneath the Atlas Mountains comes from (a) a mantle upwelling due to the delamination of the lithospheric root of the Atlas Mountains (Ramdani, 1998), or (b) a new baby plume activated in the region that does not require a delaminated lithosphere corridor beneath the mountains (Fullea et al., 2010; Lustrino & Wilson, 2007). Correspondingly, the UpW model is composed solely of vertically aligned SFD of anisotropy (Figure 2). We expect a null FPD of SWS within the volume of the anisotropy model, as its SFD is aligned vertically (subparallel to the ray path).

3.1.2. Edge-Driven Convection (EDC)

For the EDC model representing small-scale EDC in the mantle between the West African Craton and Atlas lithosphere (Fullea et al., 2010; Kaislaniemi & van Hunen, 2014; Manjón-Cabeza Córdoba & Ballmer, 2021; Missenard & Cadoux, 2012), we implemented SFD to be vertically aligned for the upwelling and/or downwelling portion of the EDC in the northwest and southeast of the Moroccan Atlas (Figure 2 and Figure S3 in Supporting Information S1). For the horizontally circulating portion, considering the location of the West African cratonic edge, the SFD is aligned at -45° to the north (azimuth of SFD), as previous studies have suggested (Missenard & Cadoux, 2012).

3.1.3. Lateral Conduit (Lateral)

The model Lateral reflects the lateral motion of the mantle material from the Canary Plume toward the Alboran Sea. As mentioned in Section 1.1, previous studies show that the volcanic rocks from the Atlas Mountains share similar geochemical properties with ones from Canary Plume (Anguita & Hernán, 2000; Duggen et al., 2009; Lustrino & Wilson, 2007) while the FPD of SWS observations aligns well with the moving direction of plume material from the Canary Islands to the Atlas Mountains (Buontempo et al., 2008; Diaz et al., 2010; Miller & Becker, 2014; Miller et al., 2013). As the hypothesis is supported by the observed SWS, we interpolate the observed FPD of the SWS (Diaz et al., 2010, 2015; Miller et al., 2013) into a fine grid to reflect the change in FPD (Figure 1b) for its azimuth. Since it represents the lateral (sub-horizontal) travel of the mantle material, all of the SFDs are subparallel to the surface (no dip).

3.1.4. One Upwelling Column (OneStem)

The difference between models Lateral and OneStem is that OneStem has an upwelling column ("stem") reflecting a localized upwelling beneath the Middle Atlas. Sun et al. (2014) suggested the presence of a low-velocity column extending to a depth of ~ 200 km beneath the Middle Atlas. They suggested the upwelling of mantle material directly below the mountains as a cause of the low-velocity anomalies and it contributes to the high topography in addition to suction due to the rollback of the western Mediterranean Canary Plume moved laterally. The *P*-wave travel-time tomography models of Civiero et al. (2018) also showed low-velocity columns beneath the Atlas Mountains, which branch out from the Canary Plume in the mantle transition zone. To reflect the low-velocity column found beneath the Middle Atlas, we attached an upwelling stem to the model Lateral. The column (upwelling stem) extends to a depth of ~ 200 km beneath the Middle Atlas and the SFD of the stem is vertically aligned.

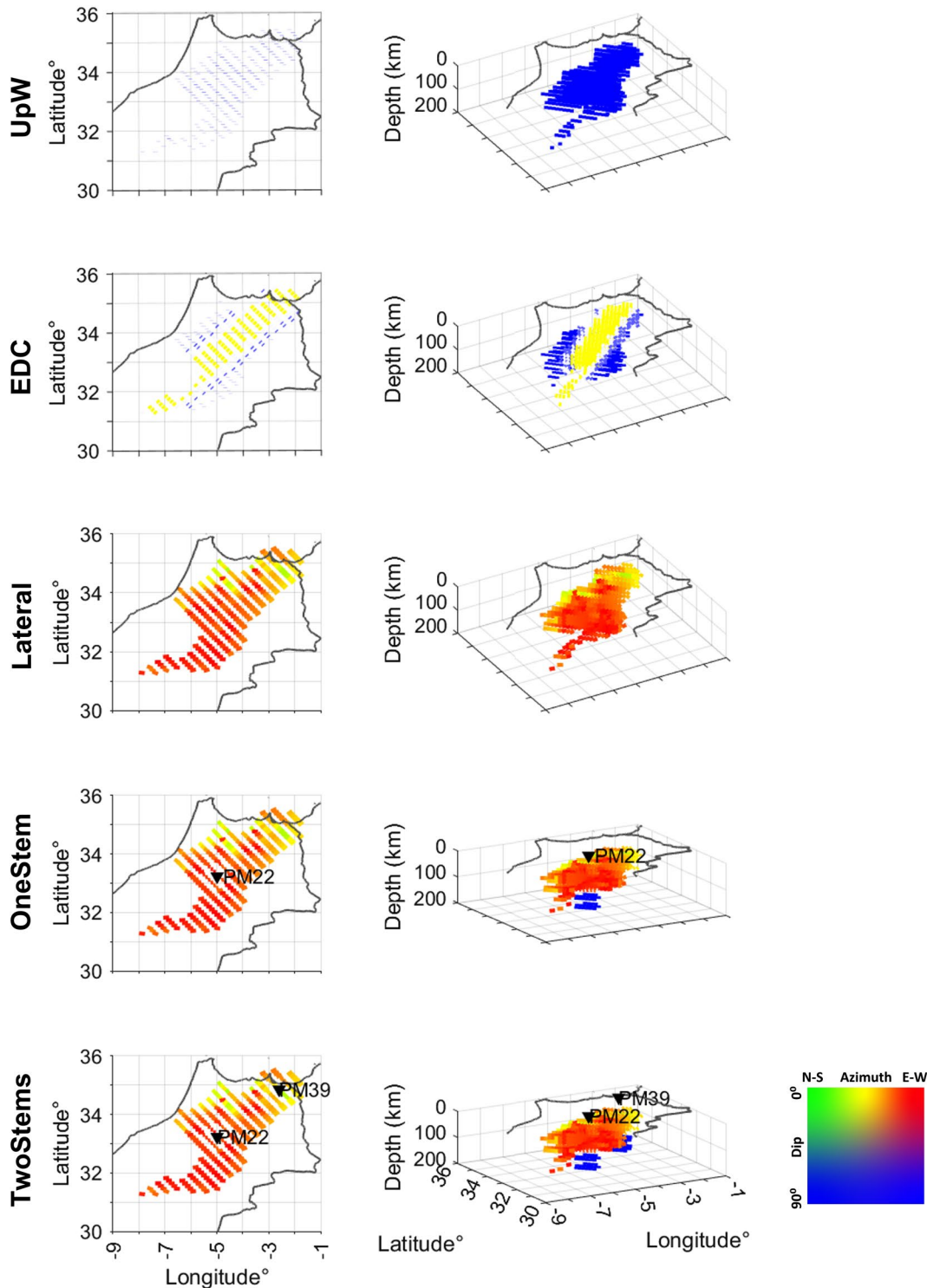


Figure 2. Five anisotropic models used in this study. Each model is placed below the High Atlas, the Middle Atlas, and northeast (NE) Morocco (the study region shown in Figure 1c) at 60–160 km depth except for OneStem and TwoStems where the stem portions extend to 200 km depth. The shape of anisotropy models is the same as the shape of low-velocity anomalies that are $\leq -2.0\%$ of dV_p/V_p for 60–160 km in the isotropic tomography images. The first column shows the map views while the second column shows the three-dimensional view of the five anisotropy models. The length of the bar represents the field of anisotropy. The orientation of the bar represents the seismically fast direction (SFD) of the anisotropy model and is colored by azimuth and dip as shown on the color scale on the right bottom. When SFD has no dip and the azimuth of SFD is oriented in N-S, it would be colored in green; in E-W, it would be colored in red. The color of SFD would be blue when it is vertically aligned (dip = 90°) regardless of the azimuth. For the detailed zoom-in view, refer to Figure S3 in Supporting Information S1. PM22 and PM39 are seismic stations centered at 33.30°N , 5.11°W for the Middle Atlas and 34.89°N , 2.61°W for the NE Morocco, respectively.

3.1.5. Two Upwelling Columns (TwoStems)

Based on receiver functions, Miller et al. (2015) further suggested another upwelling low-velocity structure near the Alboran Sea. They understood it as mantle material of the Canary Plume that was deflected toward the Alboran Sea due to mantle flow and eventually branched out as small-scale upwelling columns. Consequently, compared with the OneStem model, the TwoStems model has an additional upwelling column beneath NE Morocco that also extends to ~200 km deep. The SFD of the upwelling columns is also vertical.

3.2. Shape of Anisotropy Models (Spatial Distribution)

To explore the contribution of seismic anisotropy to the low-velocity anomalies in Morocco, we hypothetically assumed that the low-velocity anomalies, which are slower than 2% P -wave velocity perturbation (dV_p/V_p) below lithosphere of the Moroccan Atlas and NE Morocco, solely originate from seismic anisotropy (Figure 1c and Figure S2 in Supporting Information S1). All of our anisotropy models were placed where we find the images of low-velocity anomalies slower than 2% in the isotropic tomography ("Spatial distribution" in Table 1). The spatial distribution of the anisotropy model at each depth slice is contained by the -2% dV_p/V_p anomaly contour at that depth (Figure S2 in Supporting Information S1).

3.3. Placement Depth of Anisotropy Models (Depth Distribution)

As we found slow velocity anomalies ($\leq -2\%$ dV_p/V_p) at 60–160 km depth, we placed the anisotropy models within 60–160 km depth ("depth distribution" in Table 1) (Figure S2 in Supporting Information S1), except for anisotropy models OneStem and TwoStems. The anisotropy model OneStem has a stem portion representing the uprising hot mantle column beneath the Middle Atlas (Sun et al., 2014) whereas the TwoStems model has an additional stem beneath NE Morocco (Miller et al., 2015) (Figure 2 and Figure S3 in Supporting Information S1). The stems are at 160–200 km depth and are represented by cylindrical columns with 100 km diameters specifically centered at station PM22 (33.30°N, 5.11°W) for the Middle Atlas region in both the OneStem and TwoStems models. Whereas, TwoStems has another stem centered at station PM39 (34.89°N, 2.61°W) in NE Morocco (i.e., the difference between OneStem and TwoStems is that TwoStems has one more stem centered at station PM39 in the NE Morocco region).

3.4. Anisotropy Field (Magnitude of Anisotropy)

The magnitude of anisotropy in the models attempted to reproduce the observed 1.0-s delay time, which is the mean observed delay time within the study area, from 60 to 160 km depth for a vertically incident S -wave (black-dashed box in Figure 1c) (Diaz et al., 2010, 2015; Miller et al., 2013) except for the stems of the OneStem and TwoStems anisotropy models. As stems extend to a depth of 200 km, the stem portions are set to reproduce a 1.0-s delay from a depth of 60–200 km. Although we expect null SWS observation where SFDs are vertically aligned, and so have no constraint on the magnitude of anisotropy, we assume that the mantle experiences a comparable amount of shear in regions with horizontal and vertical SFDs and thus for all regions use the anisotropy fraction that would result in the observed splitting time over the assumed thickness if the SFD was horizontal. We note that the observed splitting time from NE Morocco (southern Alboran Sea) is larger than 1.0 s with the change in the complex FPD. Previous studies (e.g., Diaz et al., 2010, 2015; Lee et al., 2021; Miller et al., 2013) have suggested that toroidal mantle flows around the Alboran slab may contribute to the large and complex SWS observed in the region. In other words, the toroidal mantle flow may have contributed to the observed SWS. However, SWS is an integrated effect of anisotropy along the ray path and, consequently, the observed regional SWS does not tell how much of the splitting time comes from the toroidal mantle flow. Therefore, despite the observed SWS time being larger in NE Morocco than in the other two regions, we set the anisotropy field to reproduce the mean of the observed SWS time (1.0 s) from the entire study area for NE Morocco. To convert the observed SWS time into anisotropy fraction for P -wave tomography, we multiplied the S -wave velocity anisotropy (AVs) by a factor of 1.51 to obtain P -wave velocity anisotropy (AVp) (i.e., $AV_p/AV_s = 1.51$) based on elastic tensors of natural peridotite samples (Hammond & Toomey, 2003; Kern, 1993). To reproduce 1.0-s SWS time, the estimated magnitude of anisotropy was 6.7% for the 1.0-s delay from 60 to 160 km, while it was 4.8% for the stem portions of OneStem and TwoStems from 60 to 200 km depth.

Table 2
Results of Isotropy and the Five Anisotropy Models

Model name	Isotropy	UpW	EDC	Lateral	OneStem	TwoStems
Travel-time residual (s)	0.245	0.253	0.258	0.247	0.248	0.249
Model norm 60–200 km	0.560	0.765	0.617	0.463	0.498	0.503
60–600 km	0.655	0.847	0.726	0.579	0.604	0.608

3.5. Quantitative Comparison of Anisotropy Models

To quantify the influence of the hypothetical anisotropy models, we compared (a) the misfit to the observed travel-time delays (root-mean-squared (RMS) travel-time residuals) and (b) the change in the velocity anomalies in the final tomographic result (model norm). As unaccounted-for anisotropy can introduce artificial velocity anomalies in isotropic tomography inversions (e.g., Bezada et al., 2016; Blackman & Kendall, 1997; Blackman et al., 1996; Kendall, 1994; Lloyd & Van der Lee, 2008; Menke, 2015; Sobolev et al., 1999; VanderBeek & Faccenda, 2021), we expect a reduction in the model norm (i.e., fewer apparent velocity anomalies) and in the travel-time residual misfit, if our anisotropy model is a good approximation of the true anisotropy in the mantle even when the azimuth of the anisotropy model is not exact (Bezada et al., 2016). Note that the inclusion of arbitrary anisotropy does not automatically result in a decrease of the isotropic velocity model norm, since hypothetical anisotropy that is inconsistent with the observations will instead result in additional isotropic artifacts.

The misfit between the observed and predicted SWS can be another valuable measure of the success of the anisotropy model since some of the hypothetical anisotropy models may be inconsistent with the SWS observations. Therefore, we compared the fit of the anisotropy models to the observed SWS by utilizing the MATLAB Seismic Anisotropy Toolbox (MSAT) (Walker & Wookey, 2012). However, in this study, the SFD and anisotropy fractions of the hypothetical anisotropy models are designed to be consistent with the SWS, so the misfit to SWS information is not diagnostic. Thus, we do not rely on SWS misfit to compare the anisotropy models. For completeness, we include further details of the SWS misfit results in Figure S4 in Supporting Information S1.

4. Results

4.1. Travel-Time Residual (Data Misfit) and Model Norm

We find insignificant changes in the RMS of the travel-time residuals when we consider different anisotropy models compared with the isotropic model after the inversion (Table 2). For the Moroccan Atlas and NE Morocco (black dashed box in Figure 1c), the travel-time residuals of the isotropic velocity model were 0.245 s, while they were 0.253, 0.258, 0.247, 0.248, and 0.249 s for UpW, EDC, Lateral, OneStem, and TwoStems, respectively. Although the changes are very small, the travel-time residuals of EDC increase the most (by ~5%) compared with that of the isotropic case.

Meanwhile, we found moderate changes in the model norm within the study area at depths of 60–200 km. We note that the anisotropy models UpW, EDC, and Lateral are placed at 60–160 km, but we compare the model norm within 60–200 km depth for the study region (black dashed box in Figure 1c), as the stems of OneStem and TwoStems extend to 200 km depth. We found a reduction in the model norm by including the anisotropy model Lateral (0.463), OneStem (0.498), and TwoStems (0.503) compared with the model norm of isotropy (0.560) (Table 2). In contrast, we found an increase in the model norm for UpW (0.765) and EDC (0.617). As a result, compared to Isotropy, the model norm of UpW has increased by ~35%, while that of Lateral has decreased the most by ~15%. Simultaneously, we found a similar result for the change in the model norm at 60–600 km depth. While the model norm of the isotropic model is 0.655, the model norms for Lateral (0.579), OneStem (0.604), and TwoStems (0.608) are decreased. In contrast, the model norms for UpW (0.847) and EDC (0.726) were higher than that of the isotropic model.

4.2. P-Wave Travel-Time Tomography

Compared with the isotropic tomography images (model Isotropy) of the lithosphere of the High Atlas, we found no considerable differences in the low-velocity anomalies when we included the anisotropy models. In the High

Atlas region of UpW, the model shows an increase in low-velocity anomalies by $\sim 0.5\%$ dV_p/V_p at shallow depths (<200 km) (“H” in Figures 3g–3l).

In the Middle Atlas region, compared with model Isotropy, we also found minor changes in the low-velocity anomalies at the shallower depths (<90 km), except for model UpW, which showed an increase in low-velocity anomalies by $\sim 0.5\%$ (“M” in Figures 3g–3l). At the deeper depths (90–160 km), the Lateral and EDC show a $\sim 2\%$ reduction in the low-velocity anomalies, whereas UpW shows more than a 1.5% increase in the low-velocity anomalies (Figure 3, Figure S5 and S6 in Supporting Information S1). However, the EDC model shows an increase in the low-velocity anomalies in the northwestern region of the Middle Atlas, where the model EDC has SFD aligned vertically, reflecting the upwelling portion of mantle convection (Figures 2 and 3c, Figures S3 and S5 in Supporting Information S1). At a depth of 300–400 km below the Middle Atlas region, we observed a blob of a high-velocity volume from both the isotropic and anisotropic models (“D” in Figures 3g–3l).

Among the three regions of High Atlas, Middle Atlas, and NE Morocco, we observed the most significant changes in the velocity anomalies below NE Morocco (Figure 3, Figures S5 and S6 in Supporting Information S1). For instance, for all models except for the UpW and deeper depths of the TwoStems model (125–200 km depth), we found a decrease in low-velocity anomalies. Among the anisotropic models that show a decrease in the low-velocity anomalies, the model Lateral shows the greatest reduction of up to $\sim 2\%$ in the low-velocity anomalies below 90 km depth. The reduction found from the low-velocity anomalies at 90 km depth and deeper is $\sim 2\%$ for the model OneStem. Model EDC also indicates a $\sim 2\%$ reduction in the low-velocity anomalies for the depths above 90 km; however, it showed a $\sim 1\%$ reduction in the velocity anomalies below 90 km depth (Figure S5 in Supporting Information S1). Model UpW and TwoStems (an extra stem portion in NE Morocco in comparison to OneStem) present an extension of the low-velocity column to a depth of ~ 300 km, while this low-velocity column is greatly reduced in EDC, Lateral, and OneStem, compared with the isotropic model (Figure 3, Figures S5 and S6 in Supporting Information S1).

5. Discussion

5.1. Analyses of Travel-Time Residuals and Model Norm

Jointly considering the changes in the travel-time residuals and model norm, we found that model Lateral is the best approximation of the anisotropic structure among the five anisotropy models. As shown in Bezada et al. (2016), a good approximation of the anisotropy structure in tomographic inversion results in reductions in the travel-time residuals and model norm. We find insignificant changes in the travel-time residuals of anisotropy models (~ 0.01 s and $<5\%$) compared with model Isotropy. Although the change is very small, we find the closest time residuals from Lateral (0.247 s) to Isotropy (0.245 s) among the anisotropic models, followed by OneStem (0.248 s) and TwoStems (0.249 s) (Table 2 and Figure 4), while we observe the most increased residuals from model EDC (0.258 s). Since none of our anisotropy models reduced the travel-time residual significantly, further investigations on the insensitivity of travel-time residuals to the *a priori* anisotropic models would be very useful, but this is beyond the scope of this study.

In terms of the model norm for the depth in which anisotropy models are placed (60–200 km), including model Lateral reduces the model norm the most, by over 15%, compared with model Isotropy. We found a reduction in model norm from OneStem (0.498 and $\sim 10\%$) and TwoStems (0.503 and $\sim 10\%$). In contrast, we find the largest increase from UpW (0.765) by $\sim 37\%$, followed by EDC (0.617), which shows a $\sim 10\%$ increase. The change in the model norm at depths of 60–660 km was similar to that from a depth of 60–200 km. Model Lateral (0.579) shows the largest reduction in the model norm ($\sim 12\%$), whereas models OneStem (0.604) and TwoStems (0.608) show reductions of $\sim 8\%$ and $\sim 7\%$, respectively. Similar to the result of 60–200 km depth interval, the norms of UpW (0.847) and EDC (0.726) increased by 30% and 11%, respectively.

For model OneStem, we find a slightly larger model norm, while the travel-time residuals demonstrate a marginal difference from those of model Lateral. This suggests that the OneStem model may be a good approximation to the anisotropy structure in the study region. At the same time, our results strongly suggest that UpW and EDC are not good approximations of the anisotropy structure in the region, as neither the travel-time residuals nor the model norm is improved over the isotropic model. Consequently, model Lateral represents lateral travel of the Canary Plume while OneStem comes with one stem attached to the model Lateral, we learn that the current

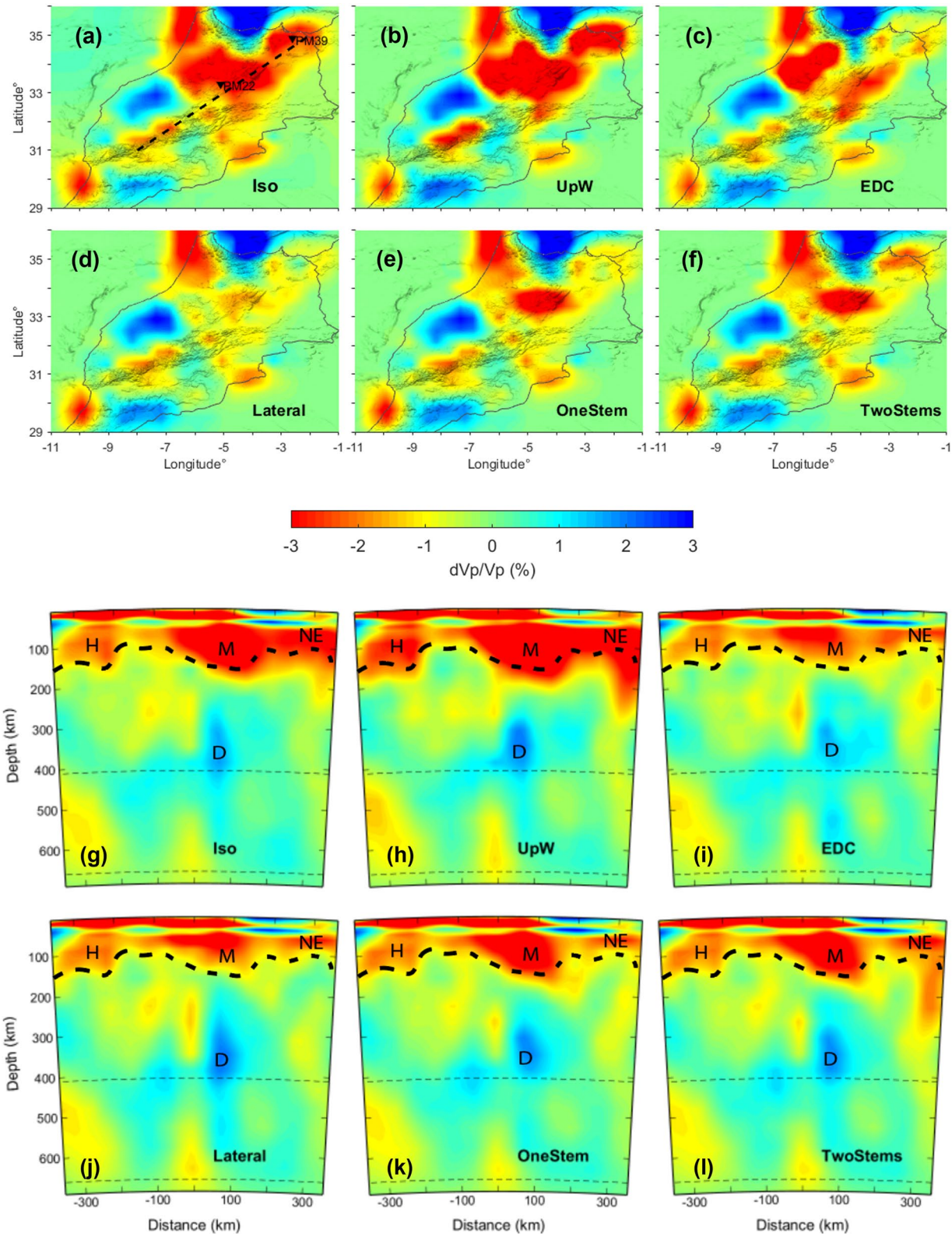


Figure 3. (a–f) Show tomographic slices at a 125 km depth from the isotropic and anisotropic models. The black dashed line in panel (a) represents the cross-sectional line ($[31^{\circ}\text{N}, 8^{\circ}\text{W}]\text{--}[35^{\circ}\text{N}, 2^{\circ}\text{W}]$) for panels (g–l), which shows the cross-sectional views of each model. The black thick dashed lines in panels (g–l) are the bases of the low-velocity anomalies observed from the (j) lateral model. The regions denoted by “H,” “M,” and “NE” in panels (g–l) are High Atlas, Middle Atlas, and NE Morocco, respectively. The region denoted by “D” may present the delaminated lithosphere discussed in Section 5.3. The (a–f) in $\pm 5\%$ dVp/Vp color scale can be found in Figure S6 in Supporting Information S1.

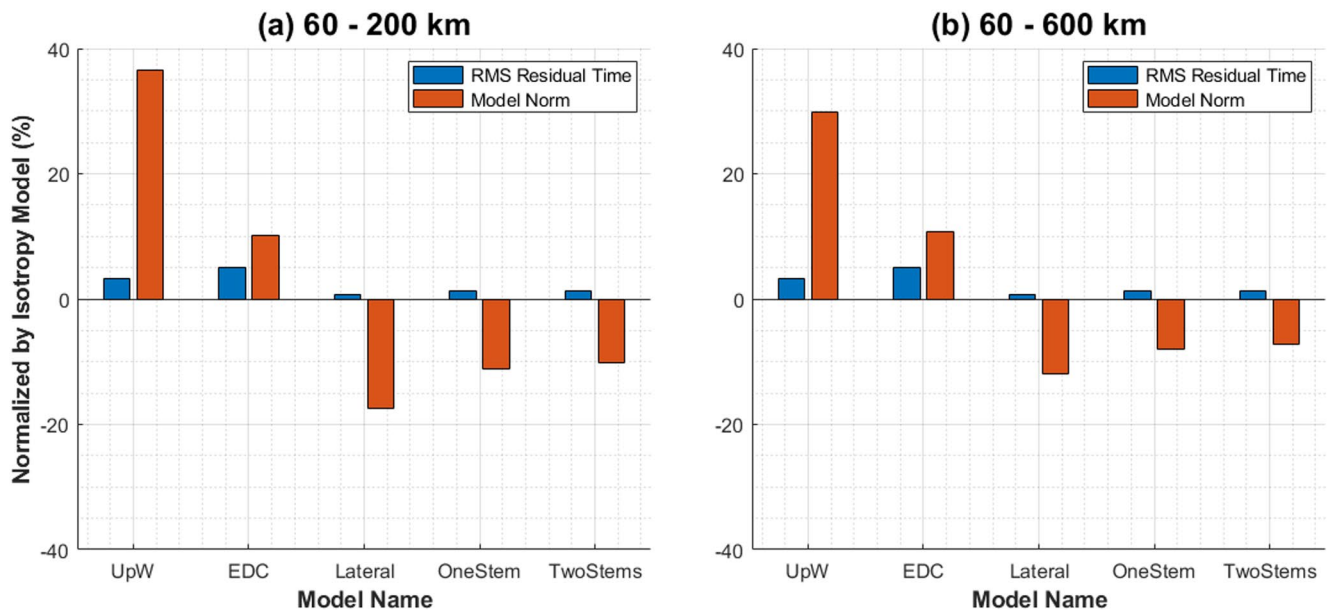


Figure 4. Bar graphs that show the changes in root-mean-squared travel-time residuals (blue) and model norm (red) in % compared to the isotropy model within the study region at (a) 60–200 depth and (b) 60–600 km depth.

configuration of the mantle is most consistent with the lateral displacement of mantle material of the Canary Plume as an origin of the low-velocity anomalies found beneath Morocco (Figure 6).

5.2. Origin of the Low-Velocity Anomalies

Our results show that the higher reduction in the travel-time residuals and the model norm is accompanied by a reduction in the low-velocity anomalies beneath the Middle Atlas and NE Morocco, specifically for depths greater than 90 km (Figure 5, Figures S5 and S7 in Supporting Information S1). The reduction in the low-velocity anomalies is only observed in the anisotropy models whose SFD are aligned subparallel to the surface (Lateral, horizontal convection portion of EDC, and OneStem beneath NE Morocco), not with the SFD aligned perpendicular to the surface (UpW, vertical convection portion of EDC, and the stem locations of OneStem and TwoStems). Compatible with these results, this may imply that the mantle flow is currently configured parallel to the surface (or plate) in the region. Therefore, instead of a regional upwelling (Ebinger & Sleep, 1998; Fullea et al., 2010; Kaislaniemi & van Hunen, 2014; Lustrino & Wilson, 2007; Missenard & Cadoux, 2012), our results suggest that the mantle material of the Canary Plume moving toward the Alboran Sea may have entrained the surrounding mantle and consequently developed anisotropy, whether through a lateral conduit only (Anguita & Hernán, 2000; Duggen et al., 2009) or with a local upwelling plume branch (Civiero et al., 2018; Miller & Becker, 2014; Miller et al., 2015; Sun et al., 2014). We should note that the shape of the low-velocity anomalies at the depths of 60–160 km (the contour of -2% dV_p/V_p) of isotropic and anisotropic tomography images is discrete and does not appear to be a continuous conduit extending from the Canary Hotspot to the Alboran Sea. Nonetheless, based on our quantitative result (Section 5.1), it is hard to prefer a local upwelling plume branch (represented by model OneStem) over a lateral conduit (represented by model Lateral) for the displacement of mantle material of the Canary Plume. Additional studies on the detailed exploration of the two hypotheses will be useful. In addition, the undisturbed low-velocity anomalies below the High Atlas and at shallower depths (<90 km) of the Middle Atlas and NE Morocco, regardless of the incorporation of anisotropy, suggest that these anomalies may not solely be a product of seismic anisotropy. However, our study does not allow us to discern other possible causes (Figure 6).

5.3. High-Velocity Structure in the Deeper Depths (300–400 km) Beneath the Middle Atlas

When we compare the isotropic and five anisotropic results, we find an unchanged high-velocity anomaly below the Middle Atlas at a depth of 300–400 km (denoted as “D” in Figures 3g–3l). Similar to the unchanged

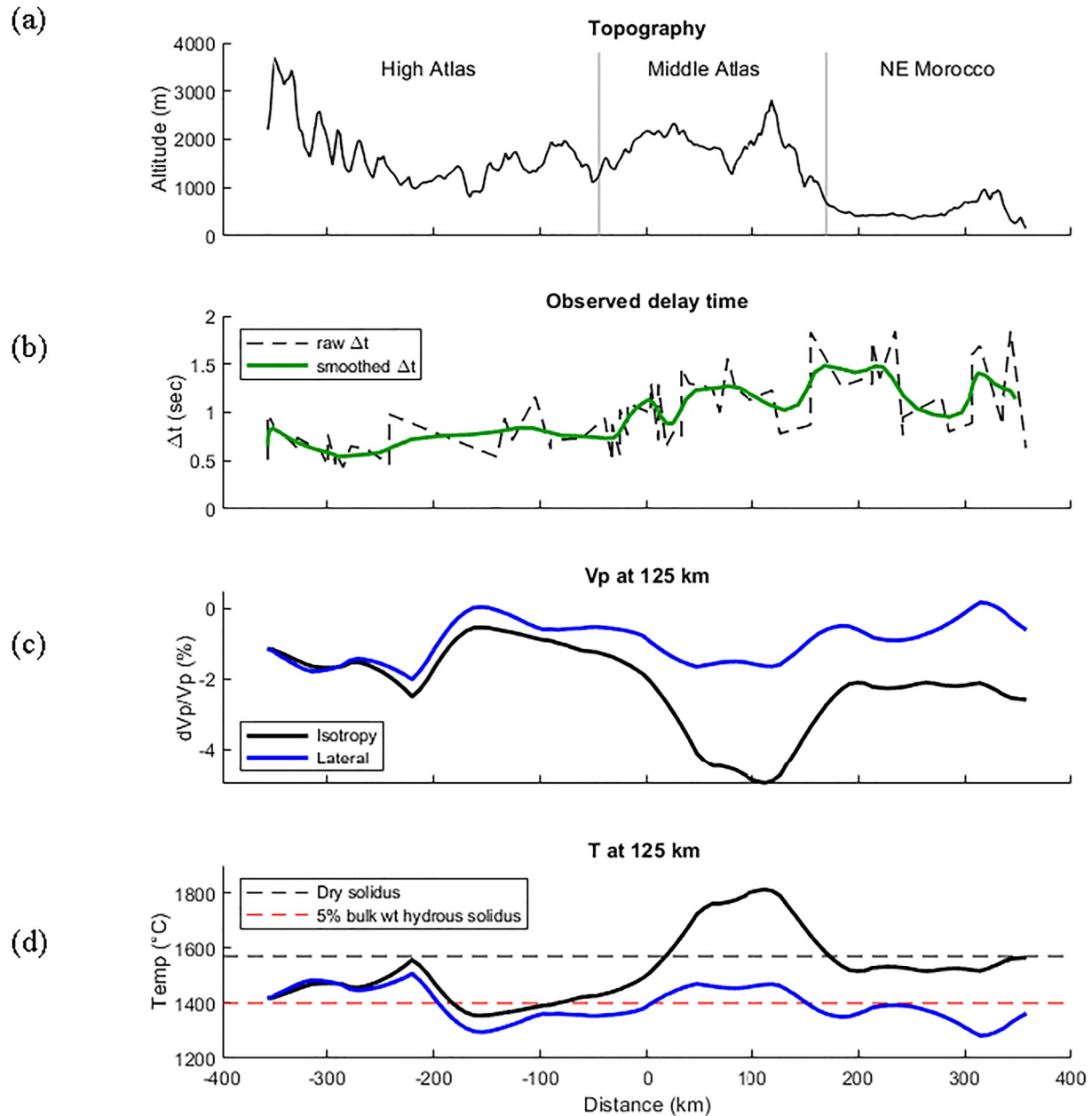


Figure 5. The change of (a) topography; (b) the observed delay time of shear wave splitting (Diaz et al., 2010; Miller et al., 2013); (c) dV_p/V_p at 125 km depth for the isotropy tomography (black line) and anisotropy tomography including model Lateral (blue line); (d) our estimated temperature from the isotropy tomography (black line) and anisotropy tomography (blue line), based on the temperature derivatives of V_p (Cammarrano et al., 2003) at 125 km (4 GPa) along with the black dashed line in Figure 3a ($[31^{\circ}\text{N}, 8^{\circ}\text{W}]-[35^{\circ}\text{N}, 2^{\circ}\text{W}]$). For (d), the dry solidus is at 1570°C (Hirschmann, 2000) and the 5-bulk-weight% hydrous solidus is at 1400°C (Katz et al., 2003).

low-velocity anomalies at shallow depths, we consider this to be a true high-velocity structure rather than an artifact of the unaccounted-for anisotropy. Bezada et al. (2014) showed the same high-velocity structure, which was interpreted as the delaminated lithosphere of the Atlas Mountains (see Bezada et al. (2014) for the details of lithospheric delamination). Although our results indicate that the mantle material from the Canary Plume could be the origin of the low-velocity anomalies beneath the Middle Atlas (<200 km), it is difficult to conclusively determine the cause of delamination. Therefore, further studies on this high-velocity volume and its origin are required.

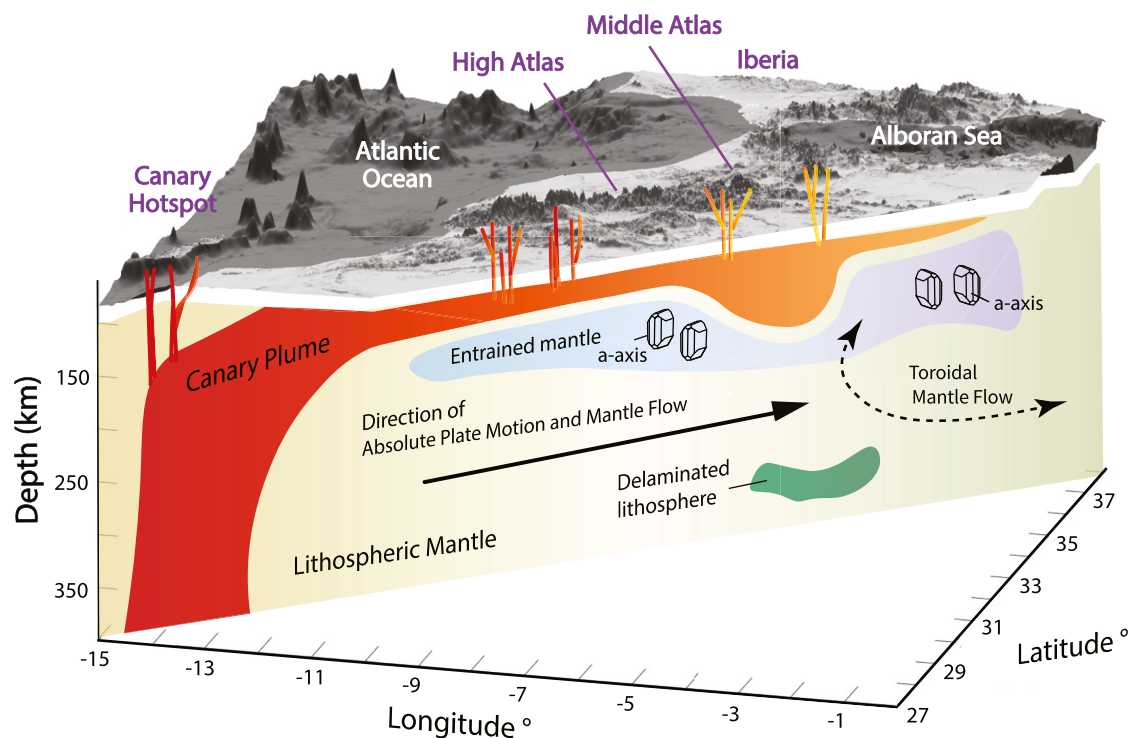


Figure 6. A schematic view for the lateral travel of the Canary Plume material. It shows that the lateral travel of the plume material of Canary Hotspot has entrained mantle beneath it, which may have developed seismic anisotropy consequently beneath the Atlas Mountains as observed by the shear wave splitting (SWS). Meanwhile, the toroidal mantle flow generated by the rollback of the Alboran slab near northeast Morocco may contribute to the seismic anisotropy observed by SWS. The plot is not on an absolute scale.

5.4. Origin of the Complex SWS in NE Morocco

Unlike the Moroccan Atlas regions, the observed SWS times in NE Morocco increase to ~ 2 s. The FPD is irregular and inconsistent with the suggested direction of mantle flow in NE Morocco (Diaz et al., 2010, 2015; Miller et al., 2013). The change in the observed SWS compared with the Moroccan Atlas region may be related more to the location of the Alboran slab below the Alboran Sea (the high-velocity anomalies found below the Alboran Sea in Figures 1c and 3a–3f, Figures S5 and S7 in Supporting Information S1) (Bezada et al., 2014; Calvert et al., 2000; Diaz et al., 2010; Miller et al., 2015) and the toroidal mantle flow due to slab rollback (Alvarez, 1982; Ayarza et al., 2005; Bezada et al., 2016; Civello & Margheriti, 2004; Faccenda & Capitanio, 2012; Hu et al., 2017; Lee et al., 2021; Long & Becker, 2010; Long & Silver, 2008; Russo & Silver, 1994). Based on our study, it is difficult to quantify the extent of anisotropy developed by the displacement of the Canary Plume and rollback of the Alboran slab. Despite the facts that (a) it has been suggested that the subduction of the Alboran slab and its retreat/rollback may have created suction of the surrounding mantle (Civiero et al., 2019; Duggen et al., 2009; Faccenna et al., 2005; Spakman et al., 2018) and (b) the moving direction of Canary Plume material is well aligned with the absolute mantle flow direction suggested by the global model of Conrad and Behn (2010), which predicts NE-SW-directed mantle flow in the study region, exploring the driving mechanism for the extensive distance ($\sim 1,500$ km) for plume travel is beyond the scope of our study.

5.5. Role of Seismic Anisotropy in Tomography for Temperature Interpretations

In addition to the effect of seismic anisotropy, seismic velocity in the mantle is sensitive to temperature, mantle composition, and the content of water, melt, and other volatiles. Among these factors, seismic velocity is often interpreted as a proxy for temperature. To explore the influence of seismic anisotropy on the interpretation of mantle conditions below the Moroccan Atlas and NE Morocco, we estimated the temperature of the mantle from the velocity anomalies based on the V_p temperature derivatives with the V_p of Cammarano et al. (2003). We chose the model Lateral for comparison with model Isotropy, as our results suggest that it is the best approximation

of the true anisotropy structure in the region among the anisotropy models tested. To keep the pressure constant at ~ 4 GPa, we choose the 125-km depth slice of our velocity model, where the change in velocity anomalies is significant between the isotropic and anisotropic tomography models (Figures 3–5, and Figure S7 in Supporting Information S1). At this depth, the approximate dry solidus of peridotite is $\sim 1570^\circ\text{C}$ (Hirschmann, 2000), whereas that of 5-bulk-wt-% hydrous peridotite is $\sim 1400^\circ\text{C}$ (Katz et al., 2003). We also assume that the ambient temperature of the mantle at this depth is $\sim 1300^\circ\text{C}$, based on a study of the MORB (Herzberg et al., 2007). At 125 km below the High Atlas, the estimated temperature is 1300°C – 1500°C (Figure 5) for both models Isotropy and Lateral. Depending on the water content of the mantle at this depth, this implies that melt may be present. For the Middle Atlas, the estimated temperature of the isotropic velocity anomalies was $\sim 200^\circ\text{C}$ above the dry solidus of the peridotite. Based on our study, in contrast to the isotropic temperature, the estimated temperature considering seismic anisotropy was below the dry solidus of the peridotite. Similar to the High Atlas, the presence of melt is possible for the Middle Atlas depending on the water content of the mantle; however, it is not required when anisotropy is considered. We found a similar result for the temperature conversion of seismic velocities in other studies. For instance, Sun et al. (2014) suggested that the estimated temperature of the low-velocity column found in the lithosphere below the Middle Atlas is $\sim 1500^\circ\text{C}$, which is similar to the temperatures predicted for the Atlas Mountains by Thurner et al. (2014), based on thermobarometric results (1400°C – 1500°C). More recently, Civiero et al. (2019) suggested that the temperature of the lithosphere below the Atlas Mountains is 200°C – 350°C higher than that of the adiabatic mantle at 1300°C . For NE Morocco, we found a temperature of $\sim 1530^\circ\text{C}$ in the isotropic model and $\sim 1350^\circ\text{C}$ in the anisotropic model. In other words, the presence of melt was not necessary for the anisotropic model below NE Morocco. In summary, for the isotropic model, the presence of melt is necessary for the Middle Atlas regardless of the water content of the mantle. In contrast, when anisotropy is considered, the presence of melt is not required, but possible in all regions depending on the hydration condition of the mantle. Relatively high temperatures below both the High and the Middle Atlas can be related to the recent voluminous magmatism during the 1.8–0.5 Ma (Anguita & Hernán, 2000; Duggen et al., 2009; Teixell et al., 2005). Further studies are required to better understand the relationships between the mantle temperature derived from velocity perturbations and the recent volcanic activity in the High Atlas, Middle Atlas, and NE Morocco.

6. Conclusions

Although various possible origins for low-velocity anomalies supporting the rootless Atlas Mountains in Morocco have been previously studied, a consensus has not yet been reached. Mantle flow can develop seismic anisotropy and be observed by SWS, which has been previously studied in this region. In this study, by incorporating five representative anisotropic structures (regional upwelling, EDC, lateral conduit of mantle material from the Canary Plume, and one and two upwelling branches from the Canary Plume) in the *P*-wave travel-time tomography, we examine the current configuration of the mantle to help us infer the origin of the low-velocity anomalies. From this study, we find the best result in the travel-time residuals and model norm when we incorporate the anisotropy structure representing the lateral conduit of the mantle material from the Canary Plume in the lithospheric mantle below the Atlas Mountains. We also find similar results from a model that includes a local upwelling beneath the Middle Atlas. Consequently, our results lend support to the hypothesis that mantle material from the Canary Plume is likely the origin of the low-velocity anomalies found beneath the Moroccan Atlas Mountains. In contrast, we found the least favorable results by including an anisotropy model representing regional upwelling. Simultaneously, we observed that the low-velocity anomalies in the isotropic model were partially produced by seismic anisotropy beneath the Middle Atlas and NE Morocco, and that not accounting for this anisotropy would result in a significant over-estimation of the temperature anomalies and lead to erroneous inferences about the likely melt fraction in this area.

Data Availability Statement

Data used in this study are accessible through Incorporated Research Institutions for Seismology (IRIS), Kennett et al. (1995), Diaz et al. (2010), Miller et al. (2013), Bezada et al. (2013), and Palomeras et al. (2014). MATLAB Seismic Anisotropy Toolkit (MSAT) is available through Walker and Wookey (2012).

Acknowledgments

H. Lee acknowledges the support from the National Research Foundation of Korea (NRF 2021R1A6A3A0108673611) and Y. Kim acknowledges support from the NRF grant funded by the Korean government (MSIT) (2022R1A5A1085103). This work was also partially funded by the U.S. National Science Foundation (EAR-1520695). We would like to thank Joseph Byrnes and Hyunsun Kang for the extensive discussion and comments, and also thank two anonymous reviewers for their valuable comments that helped us to improve the manuscript.

References

- Alvarez, W. (1982). Geological evidence for the geographical pattern of mantle return flow and the driving mechanism of plate tectonics. *Journal of Geophysical Research*, 87(B8), 6697–6710. <https://doi.org/10.1029/JB087iB08p06697>
- Anahnah, F., Galindo-Zaldívar, J., Chalouan, A., Pedrera, A., Ruano, P., Pous, J., et al. (2011). Deep resistivity cross section of the intraplate Atlas Mountains (NW Africa): New evidence of anomalous mantle and related Quaternary volcanism. *Tectonics*, 30(5), TC5014. <https://doi.org/10.1029/2010TC002859>
- Anderson, D. L. (1989). *Theory of the Earth*. MA Blackwell Scientific Publications.
- Anguita, F., & Hernán, F. (2000). The Canary Islands origin: A unifying model. *Journal of Volcanology and Geothermal Research*, 103(1), 1–26. [https://doi.org/10.1016/S0377-0273\(00\)00195-5](https://doi.org/10.1016/S0377-0273(00)00195-5)
- Arboleya, M. L., Teixell, A., Charroud, M., & Julivert, M. (2004). A structural transect through the High and Middle Atlas of Morocco. *Journal of African Earth Sciences*, 39(3), 319–327. <https://doi.org/10.1016/j.jafrearsci.2004.07.036>
- Ayarza, G., Alvarez-Lobato, F., Teixell, A., Arboleya, M. L., Tesón, E., Julivert, M., & Charroud, M. (2005). Crustal structure under the central High Atlas Mountains (Morocco) from geological and gravity data. *Tectonophysics*, 400(1), 67–84. <https://doi.org/10.1016/j.tecto.2005.02.009>
- Bagley, B., & Nyblade, A. A. (2013). Seismic anisotropy in eastern Africa, mantle flow, and the African superplume: Seismic anisotropy in eastern Africa. *Geophysical Research Letters*, 40(8), 1500–1505. <https://doi.org/10.1002/grl.50315>
- Barrau, G., Sigloch, K., Scholz, J.-R., Mazzullo, A., Stutzmann, E., Montagner, J.-P., et al. (2019). Large-scale flow of Indian Ocean asthenosphere driven by Réunion plume. *Nature Geoscience*, 12(12), 1043–1049. <https://doi.org/10.1038/s41561-019-0479-3>
- Beauchamp, W., Allmendinger, R. W., Barazangi, M., Demnati, A., Alji, M. E., & Dahmani, M. (1999). Inversion tectonics and the evolution of the High Atlas Mountains, Morocco, based on a geological-geophysical transect. *Tectonics*, 18(2), 163–184. <https://doi.org/10.1029/1998TC000015>
- Bezada, M. J., Faccenda, M., & Toomey, D. R. (2016). Representing anisotropic subduction zones with isotropic velocity models: A characterization of the problem and some steps on a possible path forward: Anisotropic subduction, isotropic models. *Geochemistry, Geophysics, Geosystems*, 17(8), 3164–3189. <https://doi.org/10.1002/2016GC006507>
- Bezada, M. J., Humphreys, E. D., Davila, J. M., Carbonell, R., Harnafi, M., Palomeras, I., & Levander, A. (2014). Piecewise delamination of Moroccan lithosphere from beneath the Atlas Mountains. *Geochemistry, Geophysics, Geosystems*, 15(4), 975–985. <https://doi.org/10.1002/2013GC005059>
- Bezada, M. J., Humphreys, E. D., Toomey, D. R., Harnafi, M., Dávila, J. M., & Gallart, J. (2013). Evidence for slab rollback in westernmost Mediterranean from improved upper mantle imaging. *Earth and Planetary Science Letters*, 368, 51–60. <https://doi.org/10.1016/j.epsl.2013.02.024>
- Blackman, D. K., & Kendall, J.-M. (1997). Sensitivity of teleseismic body waves to mineral texture and melt in the mantle beneath a mid-ocean ridge. *Philosophical Transactions of the Royal Society of London, Series A: Mathematical, Physical and Engineering Sciences*, 355(1723), 217–231. <https://doi.org/10.1098/rsta.1997.0007>
- Blackman, D. K., Kendall, J.-M., Dawson, P. R., Wenk, H.-R., Boyce, D., & Morgan, J. P. (1996). Teleseismic imaging of subaxial flow at mid-ocean ridges: Traveltime effects of anisotropic mineral texture in the mantle. *Geophysical Journal International*, 127(2), 415–426. <https://doi.org/10.1111/j.1365-246X.1996.tb04730.x>
- Brede, R., Hauptmann, M., & Herbig, H.-G. (1992). Plate tectonics and the intracratonic mountain ranges in Morocco—The Mesozoic—Cenozoic development of the central high Atlas and the Middle Atlas. *Geologische Rundschau*, 81(1), 127–141. <https://doi.org/10.1007/BF01764544>
- Buontempo, L., Bokelmann, G. H. R., Barrau, G., & Morales, J. (2008). Seismic anisotropy beneath southern Iberia from SKS splitting. *Earth and Planetary Science Letters*, 273(3), 237–250. <https://doi.org/10.1016/j.epsl.2008.06.024>
- Calvert, A., Sandvol, E., Seber, D., Barazangi, M., Roecker, S., Mourabit, T., et al. (2000). Geodynamic evolution of the lithosphere and upper mantle beneath the Alboran region of the western Mediterranean: Constraints from travel time tomography. *Journal of Geophysical Research*, 105(B5), 10871–10898. <https://doi.org/10.1029/2000JB900024>
- Cammarano, F., Goes, S., Vacher, P., & Giardini, D. (2003). Inferring upper-mantle temperatures from seismic velocities. *Physics of the Earth and Planetary Interiors*, 138(3), 197–222. [https://doi.org/10.1016/S0031-9201\(03\)00156-0](https://doi.org/10.1016/S0031-9201(03)00156-0)
- Chang, S.-J., & Van der Lee, S. (2011). Mantle plumes and associated flow beneath Arabia and East Africa. *Earth and Planetary Science Letters*, 302(3–4), 448–454. <https://doi.org/10.1016/j.epsl.2010.12.050>
- Christensen, N. I. (1984). The magnitude, symmetry and origin of upper mantle anisotropy based on fabric analyses of ultramafic tectonites. *Geophysical Journal International*, 76(1), 89–111. <https://doi.org/10.1111/j.1365-246X.1984.tb05025.x>
- Civello, S., & Margheriti, L. (2004). Toroidal mantle flow around the Calabrian slab (Italy) from SKS splitting. *Geophysical Research Letters*, 31(10), L10601. <https://doi.org/10.1029/2004GL019607>
- Civiero, C., Custódio, S., Neres, M., Schlaphorst, D., Mata, J., & Silveira, G. (2021). The role of the seismically slow Central-East Atlantic anomaly in the Genesis of the Canary and Madeira volcanic provinces. *Geophysical Research Letters*, 48(13), e2021GL092874. <https://doi.org/10.1029/2021GL092874>
- Civiero, C., Custódio, S., Rawlinson, N., Strak, V., Silveira, G., Arroucau, P., & Corela, C. (2019). Thermal nature of mantle upwellings below the Ibero-western Maghreb region inferred from teleseismic tomography. *Journal of Geophysical Research: Solid Earth*, 124(2), 1781–1801. <https://doi.org/10.1029/2018JB016531>
- Civiero, C., Strak, V., Custodio, S., Silveira, G., Rawlinson, N., Arroucau, P., & Corela, C. (2018). A common deep source for upper-mantle upwellings below the Ibero-western Maghreb region from teleseismic P-wave travel-time tomography. *Earth and Planetary Science Letters*, 499, 157–172. <https://doi.org/10.1016/j.epsl.2018.07.024>
- Conrad, C. P., & Behn, M. D. (2010). Constraints on lithosphere net rotation and asthenospheric viscosity from global mantle flow models and seismic anisotropy. *Geochemistry, Geophysics, Geosystems*, 11(5), Q05W05. <https://doi.org/10.1029/2009GC002970>
- DePaolo, D. J., & Manga, M. (2003). Deep origin of hotspots—The mantle plume model. *Science*, 300(5621), 920–921. <https://doi.org/10.1126/science.1083623>
- Diaz, J., Gallart, J., Morais, I., Silveira, G., Pedreira, D., Pulgar, J. A., et al. (2015). From the Bay of Biscay to the High Atlas: Completing the anisotropic characterization of the upper mantle beneath the westernmost Mediterranean region. *Tectonophysics*, 663, 192–202. <https://doi.org/10.1016/j.tecto.2015.03.007>
- Diaz, J., Gallart, J., Villaseñor, A., Mancilla, F., Pazos, A., Córdoba, D., et al. (2010). Mantle dynamics beneath the Gibraltar Arc (western Mediterranean) from shear-wave splitting measurements on a dense seismic array. *Geophysical Research Letters*, 37(18), L18304. <https://doi.org/10.1029/2010GL044201>
- Duggen, S., Hoernle, K. A., Hauff, F., Klügel, A., Bouabdellah, M., & Thirlwall, M. F. (2009). Flow of Canary mantle plume material through a subcontinental lithospheric corridor beneath Africa to the Mediterranean. *Geology*, 37(3), 283–286. <https://doi.org/10.1130/G25426A.1>
- Eberhart-Phillips, D., & Henderson, C. M. (2004). Including anisotropy in 3-D velocity inversion and application to Marlborough, New Zealand. *Geophysical Journal International*, 156(2), 237–254. <https://doi.org/10.1111/j.1365-246X.2003.02044.x>

- Ebinger, C. J., & Sleep, N. H. (1998). Cenozoic magmatism throughout east Africa resulting from impact of a single plume. *Nature*, 395(6704), 788–791. <https://doi.org/10.1038/27417>
- Faccenda, M., & Capitanio, F. A. (2012). Development of mantle seismic anisotropy during subduction-induced 3-D flow. *Geophysical Research Letters*, 39(11). <https://doi.org/10.1029/2012GL051988>
- Faccenda, M., & Capitanio, F. A. (2013). Seismic anisotropy around subduction zones: Insights from three-dimensional modeling of upper mantle deformation and SKS splitting calculations. *Geochemistry, Geophysics, Geosystems*, 14(1), 243–262. <https://doi.org/10.1002/ggge.20055>
- Faccenna, C., Civetta, L., D'Antonio, M., Funicello, F., Margheriti, L., & Piromallo, C. (2005). Constraints on mantle circulation around the deforming Calabrian slab. *Geophysical Research Letters*, 32(6), L06311. <https://doi.org/10.1029/2004GL021874>
- Fouch, M. J., & Rondenay, S. (2006). Seismic anisotropy beneath stable continental interiors. *Physics of the Earth and Planetary Interiors*, 158(2), 292–320. <https://doi.org/10.1016/j.pepi.2006.03.024>
- French, S. W., & Romanowicz, B. (2015). Broad plumes rooted at the base of the Earth's mantle beneath major hotspots. *Nature*, 525(7567), 95–99. <https://doi.org/10.1038/nature14876>
- Frizon de Lamotte, D., Bezard, B. S., Bracène, R., & Mercier, E. (2000). The two main steps of the Atlas building and geodynamics of the western Mediterranean. *Tectonics*, 19(4), 740–761. <https://doi.org/10.1029/2000TC900003>
- Fuller, J., Fernández, M., Afonso, J. C., Vergés, J., & Zeyen, H. (2010). The structure and evolution of the lithosphere–asthenosphere boundary beneath the Atlantic–Mediterranean Transition Region. *Lithos*, 120(1–2), 74–95. <https://doi.org/10.1016/j.lithos.2010.03.003>
- Fuller, J., Fernández, M., & Zeyen, H. (2008). FA2BOUG—A FORTRAN 90 code to compute Bouguer gravity anomalies from gridded free-air anomalies: Application to the Atlantic-Mediterranean transition zone. *Computers & Geosciences*, 34(12), 1665–1681. <https://doi.org/10.1016/j.cageo.2008.02.018>
- Fuller, J., Fernández, M., Zeyen, H., & Vergés, J. (2007). A rapid method to map the crustal and lithospheric thickness using elevation, geoid anomaly and thermal analysis. Application to the Gibraltar Arc System, Atlas Mountains and adjacent zones. *Tectonophysics*, 430(1), 97–117. <https://doi.org/10.1016/j.tecto.2006.11.003>
- Füri, E., Hilton, D. R., Murton, B. J., Hémond, C., Dymont, J., & Day, J. M. D. (2011). Helium isotope variations between Réunion Island and the Central Indian Ridge (17°–21°S): New evidence for ridge–hot spot interaction. *Journal of Geophysical Research*, 116(B2), B02207. <https://doi.org/10.1029/2010JB007609>
- Gomez, F., Allmendinger, R., Barazangi, M., Er-Raji, A., & Dahmani, M. (1998). Crustal shortening and vertical strain partitioning in the Middle Atlas Mountains of Morocco. *Tectonics*, 17(4), 520–533. <https://doi.org/10.1029/98TC01439>
- Hammond, W. C., & Toomey, D. R. (2003). Seismic velocity anisotropy and heterogeneity beneath the mantle electromagnetic and tomography experiment (MELT) region of the east Pacific rise from analysis of P and S body waves: EPR seismic velocity and anisotropy. *Journal of Geophysical Research*, 108(B4), 2176. <https://doi.org/10.1029/2002JB001789>
- Hansen, S. E., Nyblade, A. A., & Benoit, M. H. (2012). Mantle structure beneath Africa and Arabia from adaptively parameterized P-wave tomography: Implications for the origin of Cenozoic Afro-Arabian tectonism. *Earth and Planetary Science Letters*, 319–320, 23–34. <https://doi.org/10.1016/j.epsl.2011.12.023>
- Herzberg, C., Asimow, P. D., Arndt, N., Niu, Y., Leshner, C. M., Fitton, J. G., et al. (2007). Temperatures in ambient mantle and plumes: Constraints from basalts, picrites, and komatiites. *Geochemistry, Geophysics, Geosystems*, 8(2), Q02006. <https://doi.org/10.1029/2006GC001390>
- Hirschmann, M. M. (2000). Mantle solidus: Experimental constraints and the effects of peridotite composition: Mantle solidus. *Geochemistry, Geophysics, Geosystems*, 1(10), 1042. <https://doi.org/10.1029/2000GC000070>
- Hirth, G., & Kohlstedt, D. (2003). Rheology of the upper mantle and the mantle wedge: A view from the experimentalists. In J. Eiler (Ed.) *Geophysical Monograph Series*, (Vol. 138, pp. 83–105). American Geophysical Union. <https://doi.org/10.1029/138GM06>
- Hu, J., Faccenda, M., & Liu, L. (2017). Subduction-controlled mantle flow and seismic anisotropy in South America. *Earth and Planetary Science Letters*, 470, 13–24. <https://doi.org/10.1016/j.epsl.2017.04.027>
- Huang, Z., Zhao, D., & Liu, X. (2015). On the trade-off between seismic anisotropy and heterogeneity: Numerical simulations and application to Northeast Japan. *Journal of Geophysical Research: Solid Earth*, 120(5), 3255–3277. <https://doi.org/10.1002/2014JB011784>
- Humphreys, E. D., Dueker, K. G., Schutt, D. L., & Smith, R. B. (2000). Beneath Yellowstone: Evaluating plume and nonplume models using teleseismic images of the upper mantle. *Geological Society of America Today*, 10(12), 1–7.
- Ihinger, P. D. (1995). Mantle flow beneath the Pacific Plate; evidence from seamount segments in the Hawaiian-Emperor Chain. *American Journal of Science*, 295(9), 1035–1057. <https://doi.org/10.2475/ajs.295.9.1035>
- Ishise, M., & Oda, H. (2005). Three-dimensional structure of P-wave anisotropy beneath the Tohoku district, northeast Japan. *Journal of Geophysical Research*, 110(B7), B07304. <https://doi.org/10.1029/2004JB003599>
- Ismail, W. B., & Mainprice, D. (1998). An olivine fabric database: An overview of upper mantle fabrics and seismic anisotropy. *Tectonophysics*, 296(1–2), 145–157. [https://doi.org/10.1016/S0040-1951\(98\)00141-3](https://doi.org/10.1016/S0040-1951(98)00141-3)
- Ito, G., Dunn, R., Li, A., Wolfe, C. J., Gallego, A., & Fu, Y. (2014). Seismic anisotropy and shear wave splitting associated with mantle plume-plate interaction. *Journal of Geophysical Research: Solid Earth*, 119(6), 4923–4937. <https://doi.org/10.1002/2013JB010735>
- Kaislaniemi, L., & van Hunen, J. (2014). Dynamics of lithospheric thinning and mantle melting by edge-driven convection: Application to Moroccan Atlas Mountains. *Geochemistry, Geophysics, Geosystems*, 15(8), 3175–3189. <https://doi.org/10.1002/2014GC005414>
- Kaminski, É., & Ribe, N. M. (2002). Timescales for the evolution of seismic anisotropy in mantle flow. *Geochemistry, Geophysics, Geosystems*, 3(8), 1–17. <https://doi.org/10.1029/2001GC000222>
- Katz, R. F., Spiegelman, M., & Langmuir, C. H. (2003). A new parameterization of hydrous mantle melting. *Geochemistry, Geophysics, Geosystems*, 4(9), 1073. <https://doi.org/10.1029/2002GC000433>
- Kendall, J.-M. (1994). Teleseismic arrivals at a mid-ocean ridge: Effects of mantle melt and anisotropy. *Geophysical Research Letters*, 21(4), 301–304. <https://doi.org/10.1029/93GL02791>
- Kennett, B., Engdahl, E., & Buland, R. (1995). Constraints on seismic velocities in the Earth from travel-times. *Geophysical Journal International*, 122(1), 108–124. <https://doi.org/10.1111/j.1365-246X.1995.tb03540.x>
- Kern, H. (1993). P- and S-wave anisotropy and shear-wave splitting at pressure and temperature in possible mantle rocks and their relation to the rock fabric. *Physics of the Earth and Planetary Interiors*, 78(3), 245–256. [https://doi.org/10.1016/0031-9201\(93\)90159-7](https://doi.org/10.1016/0031-9201(93)90159-7)
- Kerr, R. C., & Lister, J. R. (2008). Rise and deflection of mantle plume tails. *Geochemistry, Geophysics, Geosystems*, 9(10), Q10004. <https://doi.org/10.1029/2008GC003124>
- Lee, H., Bezada, M. J., & Faccenda, M. (2021). Can sub-slab low-velocity anomalies be an artifact caused by anisotropy? A case study from the Alboran slab area in the western Mediterranean. *Tectonophysics*, 819, 229080. <https://doi.org/10.1016/j.tecto.2021.229080>
- Lloyd, S. M., & Van der Lee, S. (2008). Influence of observed mantle anisotropy on isotropic tomographic models. *Geochemistry, Geophysics, Geosystems*, 9(7), Q07007. <https://doi.org/10.1029/2008GC001997>

- Long, M. D., & Becker, T. W. (2010). Mantle dynamics and seismic anisotropy. *Earth and Planetary Science Letters*, 297(3–4), 341–354. <https://doi.org/10.1016/j.epsl.2010.06.036>
- Long, M. D., & Silver, P. G. (2008). The subduction zone flow field from seismic anisotropy: A global view. *Science*, 319(5861), 315–318. <https://doi.org/10.1126/science.1150809>
- Lustrino, M., & Wilson, M. (2007). The circum-Mediterranean anorogenic Cenozoic igneous province. *Earth-Science Reviews*, 81(1–2), 1–65. <https://doi.org/10.1016/j.earscirev.2006.09.002>
- Manjón-Cabeza Córdoba, A., & Ballmer, M. D. (2021). The role of edge-driven convection in the generation of volcanism—Part 1: A 2D systematic study. *Solid Earth*, 12(3), 613–632. <https://doi.org/10.5194/se-12-613-2021>
- Maupin, V., & Park, J. (2007). Theory and observations—Wave propagation in anisotropic Media. In G. Schubert (Ed.), *Treatise on geophysics* (pp. 289–321). Elsevier. <https://doi.org/10.1016/B978-04452748-6.00007-9>
- Menke, W. (2015). Equivalent heterogeneity analysis as a tool for understanding the resolving power of anisotropic travel-time tomography. *Bulletin of the Seismological Society of America*, 105(2A), 719–733. <https://doi.org/10.1785/0120140150>
- Miller, M. S., Allam, A. A., Becker, T. W., Di Leo, J. F., & Wookey, J. (2013). Constraints on the tectonic evolution of the westernmost Mediterranean and northwestern Africa from shear wave splitting analysis. *Earth and Planetary Science Letters*, 375, 234–243. <https://doi.org/10.1016/j.epsl.2013.05.036>
- Miller, M. S., & Becker, T. W. (2014). Reactivated lithospheric-scale discontinuities localize dynamic uplift of the Moroccan Atlas Mountains. *Geology*, 42(1), 35–38. <https://doi.org/10.1130/G34959.1>
- Miller, M. S., O'Driscoll, L. J., Butcher, A. J., & Thomas, C. (2015). Imaging Canary Island hotspot material beneath the lithosphere of Morocco and southern Spain. *Earth and Planetary Science Letters*, 431, 186–194. <https://doi.org/10.1016/j.epsl.2015.09.026>
- Missenard, Y., & Cadoux, A. (2012). Can Moroccan Atlas lithospheric thinning and volcanism be induced by Edge-Driven Convection? *Terra Nova*, 24(1), 27–33. <https://doi.org/10.1111/j.1365-3121.2011.01033.x>
- Missenard, Y., Zeyen, H., Frizon de Lamotte, D., Leturmy, P., Petit, C., Sébrier, M., & Saddiqi, O. (2006). Crustal versus asthenospheric origin of relief of the Atlas Mountains of Morocco: Origin of relief in Atlas Mountains. *Journal of Geophysical Research*, 111(B3), B03401. <https://doi.org/10.1029/2005JB003708>
- Montelli, R., Nolet, G., Dahlen, F. A., & Masters, G. (2006). A catalogue of deep mantle plumes: New results from finite-frequency tomography. *Geochemistry, Geophysics, Geosystems*, 7(11), Q11007. <https://doi.org/10.1029/2006GC001248>
- Morgan, W. J. (1971). Convection plumes in the lower mantle. *Nature*, 230(5288), 42–43. <https://doi.org/10.1038/230042a0>
- Morgan, W. J. (1978). Rodriguez, Darwin, Amsterdam, A second type of hotspot Island. *Journal of Geophysical Research*, 83(B11), 5355–5360. <https://doi.org/10.1029/JB083iB11p05355>
- Nolet, G., Allen, R., & Zhao, D. (2007). Mantle plume tomography. *Chemical Geology*, 241(3–4), 248–263. <https://doi.org/10.1016/j.chemgeo.2007.01.022>
- Palomas, I., Thurner, S., Levander, A., Liu, K., Villasenor, A., Carbonell, R., & Harnafi, M. (2014). Finite-frequency Rayleigh wave tomography of the western Mediterranean: Mapping its lithospheric structure. *Geochemistry, Geophysics, Geosystems*, 15(1), 140–160. <https://doi.org/10.1002/2013GC004861>
- Piqué, A., Tricart, P., Guiraud, R., Laville, E., Bouaziz, S., Amrhay, M., & Ait Ouali, R. (2002). The Mesozoic–Cenozoic Atlas belt (North Africa): An overview. *Geodinamica Acta*, 15(3), 185–208. [https://doi.org/10.1016/S0985-3111\(02\)01088-4](https://doi.org/10.1016/S0985-3111(02)01088-4)
- Portner, D. E., Beck, S., Zandt, G., & Scire, A. (2017). The nature of subslab slow velocity anomalies beneath South America: Subslab slow velocity anomalies. *Geophysical Research Letters*, 44(10), 4747–4755. <https://doi.org/10.1002/2017GL073106>
- Ramdani, F. (1998). Geodynamic implications of intermediate-depth earthquakes and volcanism in the intraplate Atlas Mountains (Morocco). *Physics of the Earth and Planetary Interiors*, 108(3), 245–260. [https://doi.org/10.1016/S0031-9201\(98\)00106-X](https://doi.org/10.1016/S0031-9201(98)00106-X)
- Ribe, N. M., & Christensen, U. R. (1994). Three-dimensional modeling of plume-lithosphere interaction. *Journal of Geophysical Research*, 99(B1), 669–682. <https://doi.org/10.1029/93JB02386>
- Ribe, N. M., & Christensen, U. R. (1999). The dynamical origin of Hawaiian volcanism. *Earth and Planetary Science Letters*, 171(4), 517–531. [https://doi.org/10.1016/S0012-821X\(99\)00179-X](https://doi.org/10.1016/S0012-821X(99)00179-X)
- Richards, M. A., & Griffiths, R. W. (1988). Deflection of plumes by mantle shear flow: Experimental results and a simple theory. *Geophysical Journal International*, 94(3), 367–376. <https://doi.org/10.1111/j.1365-246X.1988.tb02260.x>
- Ritter, J. R. R., Jordan, M., Christensen, U. R., & Achauer, U. (2001). A mantle plume below the Eifel volcanic fields, Germany. *Earth and Planetary Science Letters*, 186(1), 7–14. [https://doi.org/10.1016/S0012-821X\(01\)00226-6](https://doi.org/10.1016/S0012-821X(01)00226-6)
- Russo, R. M., & Silver, P. G. (1994). Trench-parallel flow beneath the Nazca Plate from seismic anisotropy. *Science*, 263(5150), 1105–1111. <https://doi.org/10.1126/science.263.5150.1105>
- Sandvol, E., Seber, D., Calvert, A., & Barazangi, M. (1998). Grid search modeling of receiver functions: Implications for crustal structure in the Middle East and North Africa. *Journal of Geophysical Research*, 103(B11), 26899–26917. <https://doi.org/10.1029/98JB02238>
- Seber, D., Barazangi, M., Tadili, B. A., Ramdani, M., Ibenbrahim, A., & Sari, D. B. (1996). Three-dimensional upper mantle structure beneath the intraplate Atlas and interplate Rif Mountains of Morocco. *Journal of Geophysical Research*, 101(B2), 3125–3138. <https://doi.org/10.1029/95JB03112>
- Silver, P. G. (1996). Seismic anisotropy beneath the continents: Probing the depths of geology. *Annual Review of Earth and Planetary Sciences*, 24(1), 385–432. <https://doi.org/10.1146/annurev.earth.24.1.385>
- Sleep, N. H. (1990). Hotspots and mantle plumes: Some phenomenology. *Journal of Geophysical Research*, 95(B5), 6715. <https://doi.org/10.1029/JB095iB05p06715>
- Sleep, N. H. (2008). Channeling at the base of the lithosphere during the lateral flow of plume material beneath flow line hot spots. *Geochemistry, Geophysics, Geosystems*, 9(8), Q08005. <https://doi.org/10.1029/2008GC002090>
- Sobolev, S. V., Gréssillaud, A., & Cara, M. (1999). How robust is isotropic delay time tomography for anisotropic mantle? *Geophysical Research Letters*, 26(4), 509–512. <https://doi.org/10.1029/1998GL000206>
- Spakman, W., Chertova, M. V., van den Berg, A., & van Hinsbergen, D. J. J. (2018). Puzzling features of western Mediterranean tectonics explained by slab dragging. *Nature Geoscience*, 11(3), 211–216. <https://doi.org/10.1038/s41561-018-0066-z>
- Sun, D., Miller, M. S., Holt, A. F., & Becker, T. W. (2014). Hot upwelling conduit beneath the Atlas Mountains, Morocco. *Geophysical Research Letters*, 41(22), 8037–8044. <https://doi.org/10.1002/2014GL061884>
- Teixell, A., Arboleya, M.-L., Julivert, M., & Charroud, M. (2003). Tectonic shortening and topography in the central High Atlas (Morocco). *Tectonics*, 22(5), 1051. <https://doi.org/10.1029/2002tc001460>
- Teixell, A., Ayarza, P., Zeyen, H., Fernández, M., & Arboleya, M.-L. (2005). Effects of mantle upwelling in a compressional setting: The Atlas Mountains of Morocco. *Terra Nova*, 17(5), 456–461. <https://doi.org/10.1111/j.1365-3121.2005.00633.x>

- Teixell, A., Bertotti, G., de Lamotte, D. F., & Charroud, M. (2009). The geology of vertical movements of the lithosphere: An overview. *Tectonophysics*, 475(1), 1–8. <https://doi.org/10.1016/j.tecto.2009.08.018>
- Thoraval, C., Tommasi, A., & Doin, M.-P. (2006). Plume-lithosphere interaction beneath a fast moving plate: Plume-lithosphere interaction. *Geophysical Research Letters*, 33(1), L01301. <https://doi.org/10.1029/2005GL024047>
- Thurner, S., Palomeras, I., Levander, A., Carbonell, R., & Lee, C.-T. (2014). Ongoing lithospheric removal in the western Mediterranean: Evidence from Ps receiver functions and thermobarometry of Neogene basalts (PICASSO project). *Geochemistry, Geophysics, Geosystems*, 15(4), 1113–1127. <https://doi.org/10.1002/2013GC005124>
- Timoulali, Y., Bouiflane, M., Bouskri, G., Azguet, R., & El Fellah, Y. (2019). Lithosphere structures dynamics in the central High Atlas (Morocco) by seismic tomography and gravimetric data. *Geodesy and Geodynamics*, 10(3), 241–255. <https://doi.org/10.1016/j.geog.2019.01.005>
- Timoulali, Y., Nacer, J., Youssef, H., & Mimoun, C. (2015). Lithospheric structure in NW of Africa: Case of the Moroccan Atlas Mountains. *Geodesy and Geodynamics*, 6(6), 397–408. <https://doi.org/10.1016/j.geog.2015.12.003>
- Tommasi, A., Tikoff, B., & Vauchez, A. (1999). Upper mantle tectonics: Three-dimensional deformation, olivine crystallographic fabrics and seismic properties. *Earth and Planetary Science Letters*, 168(1), 173–186. [https://doi.org/10.1016/S0012-821X\(99\)00046-1](https://doi.org/10.1016/S0012-821X(99)00046-1)
- Toomey, D. R., Solomon, S. C., & Purdy, G. M. (1994). Tomographic imaging of the shallow crustal structure of the East Pacific Rise at 9°30'N. *Journal of Geophysical Research*, 99(B12), 24135–24157. <https://doi.org/10.1029/94JB01942>
- Trampert, J. (1998). Global seismic tomography: The inverse problem and beyond. *Inverse Problems*, 14(3), 371–385. <https://doi.org/10.1088/0266-5611/14/3/002>
- VanDecar, J. C., & Crosson, R. S. (1990). Determination of teleseismic relative phase arrival times using multi-channel cross-correlation and least squares. *Bulletin of the Seismological Society of America*, 80(1), 150–169. <https://doi.org/10.1785/BSSA0800010150>
- VanderBeek, B. P., & Faccenda, M. (2021). Imaging upper mantle anisotropy with teleseismic *P*-wave delays: Insights from tomographic reconstructions of subduction simulations. *Geophysical Journal International*, 225(3), 2097–2119. <https://doi.org/10.1093/gji/ggab081>
- Walker, A. M., & Wookey, J. (2012). MSAT—A new toolkit for the analysis of elastic and seismic anisotropy. *Computers & Geosciences*, 49, 81–90. <https://doi.org/10.1016/j.cageo.2012.05.031>
- Wilson, J. T. (1963). A possible origin of the Hawaiian Islands. *Canadian Journal of Earth Sciences*, 51(6), 863–870. <https://doi.org/10.1139/p63-094>
- Wu, H., & Lees, J. M. (1999). Cartesian parametrization of anisotropic traveltimes tomography. *Geophysical Journal International*, 137(1), 64–80. <https://doi.org/10.1046/J.1365-246X.1999.00778.X>
- Zeyen, H., Ayarza, P., Fernández, M., & Rimi, A. (2005). Lithospheric structure under the western African-European plate boundary: A transect across the Atlas mountains and the Gulf of Cadiz. *Tectonics*, 24(2), TC2001. <https://doi.org/10.1029/2004TC001639>
- Zhao, D. (2007). Seismic images under 60 hotspots: Search for mantle plumes. *Gondwana Research*, 12(4), 335–355. <https://doi.org/10.1016/j.gr.2007.03.001>
- Zhao, D., Yu, S., & Liu, X. (2016). Seismic anisotropy tomography: New insight into subduction dynamics. *Gondwana Research*, 33, 24–43. <https://doi.org/10.1016/j.gr.2015.05.008>